Supporting Information

V-shaped Pyranylidene/Triphenylamine-based Chromophores with Enhanced Photophysical, Electrochemical and Nonlinear Optical Properties

Sergio Gámez-Valenzuela,[a] David Neusser,[b] Carlos Benitez-Martin,[c,d] Francisco Najera,[c,d] Juan A. Guadix,[d,e] Carlos Moreno-Yruela,[f,g] Belén Villacampa,[h] Rocío Ponce Ortiz,[a] Sabine Ludwigs,[b] Raquel Andreu,*[f] M. Carmen Ruiz Delgado*[a]

[a] Department of Physical Chemistry, University of Malaga, Campus de Teatinos s/n, 29071, Malaga, Spain. *E-mail*: carmenrd@uma.es

[b] IPOC – Functional Polymers, Institute of Polymer Chemistry, University of Stuttgart, Pfaffenwaldring 55, D-70569 Stuttgart, Germany.

[c] Departamento de Química Orgánica, Universidad de Málaga-IBIMA, Campus de Teatinos s/n, Málaga 29071, Spain

[d] Centro Andaluz de Nanomedicina y Biotecnología-BIONAND, Parque Tecnológico de Andalucía, c/Severo Ochoa, 35, 29590 Campanillas, Málaga 29071, Spain.

[e] Departamento de Biología Animal, Facultad de Ciencias, Universidad de Málaga-IBIMA, Campus de Teatinos s/n, Málaga 29071, Spain.

[f] Instituto de Nanociencia y Materiales de Aragón (INMA)-Departamento de Química Orgánica, CSIC-Universidad de Zaragoza, Zaragoza 50009, Spain . *E-mail*: randreu@unizar.es

[g] Center for Biopharmaceuticals & Department of Drug Design and Pharmacology, Faculty of Health and Medical Sciences, University of Copenhagen, Universitetsparken 2, DK-2100 Copenhagen, Denmark.

[h] Instituto de Nanociencia y Materiales de Aragón (INMA)- Departamento de Física de la Materia Condensada, CSIC-Universidad de Zaragoza, Zaragoza 50009, Spain

Table of contents:

1.   Methodology

Experimental Details

Melting points were obtained in open capillaries and are uncorrected.

^{1}H-NMR spectra were recorded at 400 MHz; δ values are given in ppm (relative to TMS) and *J* values in Hz. The apparent resonance multiplicity is described as s (singlet), d (doublet), t (triplet), q (quartet) and m (multiplet).

MALDI-TOF Mass Spectra were recorded using dithranol as matrix; accurate mass measurements were achieved using PEG as external reference and calibrating with [PEG+Na]$^+$.
Elemental analyses were carried out with a Perkin-Elmer CHN2400 microanalyzer.

Electric field induced second harmonic generation (EFISH) measurements have been carried out using a wavelength of 1907 nm. This fundamental excitation is the output of a H$_2$ Raman shifter pumped by a Q-switched Nd:YAG laser at 1064 nm. The laser repetition rate is 10 Hz and the pulse width 8 ns. A computer controlled NLO spectrometer completes the SHG experimental set-up. The excitation beam is split in two; the less intense one is directed to a *N*-(4-nitrophenyl)-(*L*)-prolinol (NPP) powder sample whose SH signal is used as a reference in order to reduce the effects of laser fluctuations. The second one is passed through a linear (vertical) polarizer and focused into the EFISH wedge-shaped liquid cell. Voltage pulses of 5 kV and 3 μs are applied across the cell (2 mm gap between the electrodes) synchronously with the laser pulses. The harmonic signals from both the EFISH cell and the NPP reference are measured with two photomultipliers. Interference filters are used to remove the residual excitation light beyond the sample and the reference.

The molecular $\mu\beta$ values of the reported compounds have been determined in dichloromethane. Several solutions (2.6×10^{-4}–8×10^{-4} M) were measured. $\mu\beta_0$ **values** were extrapolated using a two-level dispersion model,[1] with λ_{max} corresponding to the lowest energy band. Under the same experimental conditions $\mu\beta_0$ values deduced for DR1 in dichloromethane was 510×10^{-48} esu, quite close to the value reported in the same solvent by Dirk et al.[2]

The FT-Raman spectra of pure solid were obtained with an FT-Raman accessory kit (RamII)) linked to a Bruker Vertex70 spectrometer. A continuous-wave Nd-YAG laser working at λ=1064 nm was employed for excitation, and a germanium detector operating at liquid nitrogen temperature. Raman scattering radiation was collected in a back-scattering geometry with a standard spectral resolution of 4 cm^{-1}. The power of the laser beam was kept at a level lower than 100 mW in all cases. Around 3000–4000 scans were averaged for each spectrum to optimize the signal-to-noise ratio.

FT-IR spectra of pure solid samples were recorded with a Golden Gate Single Reflection Diamond ATR System (Graseby Specac) fitted into a Bruker Vertex 70 FT-IR spectrometer with a KBr beam splitter and a DLaGTS detector. The infrared spectra were collected with a standard spectral resolution of 4 cm^{-1}. Around 64 scans were enough to obtain a hight signal to noise ratio.

Electronic absorption spectra were measured on an Agilent 8453 diode-array spectrophotometer, with a resolution of 1 nm.

Steady-state fluorescent spectra were registered on an Edinburgh FLS920 spectrofluorometer, with also resolution of 1 nm. The fluorescence quantum yields of compounds **1** and **2** were

determined in CH_2Cl_2 and toluene by comparison with cresyl violet and according to a standard protocol.[3]

Experiments under **two-photon (2P) conditions** were performed using an inverted Leica SP5 MP confocal microscope hosted at the ICTS "NANBIOSIS", more specifically by the U28 Unit of the Andalusian Centre for Nanomedicine & Biotechnology (BIONAND). This microscope is equipped with a MaiTai Ti:Sapphire HP laser (Spectra-Physics, Inc.) tunable between 690 and 1040 nm.

The two-photon absorption (2PA) cross-sections (σ_{2PA}) of compounds **1** and **2** were investigated between 700 and 1000 nm by the two-photon-induced fluorescence method.[4, 5] These compounds were dissolved in toluene and then diluted to a final concentration of 10 µM. Rhodamine B (10^{-8} M in spectroscopic grade methanol) was employed as reference under experimentally identical conditions, assuming that the fluorescence quantum yield is the same independently of the excitation process. Imaging was performed using a 10x Plan APO objective (NA 0.4) focused at the air/liquid boundary, allowing the simultaneous detection of the sample and the background fluorescence. Emission and excitation spectra data for compound and background regions of interest (ROIs) were registered using ImageJ software. Further, these spectra were measured in a laser power regime where the fluorescence was proportional to the square of the laser excitation power and using a dynamic 15 nm wide emission detection window moving in 20 steps between 400 and 700 nm. With identical settings and considerations, the 2P-excitation and 2P-excited fluorescence from the polymers of compounds **1** and **2** (noted as cl-**1** and cl-**2**) were also registered. The previous mentioned objective was used, although focusing on the deposited-sample limit within the films. The occurrence of the biphotonic process was confirmed for each case, and imaging of cl-**1** and cl-**2** was performed upon 2P-excitation at 900 and 870 nm, respectively. Fluorescence was detected between 500 nm and 700 nm in both cases.

The 2P-fluorescence properties of dyes **1** and **2** within cells were also analyzed, using a 63xPLAN APO NA 1.4 oil immersion objective. Compounds **1** and **2** were visualized upon 2P-excitation at 720 and 740 nm respectively. Fluorescence was detected in both cases between 450 nm and 700 nm using a HyD non-descanned detector.

For the "In vivo cell studies", Mouse Embryonic Fibroblast (MEF) cells were isolated from 14.5 old mouse embryos following standard protocols,[6] and were cultured in complete medium (DMEM + 10% FBS + 1% Penicillin-Streptomycin + 2 mM L-Glutamine) at 37°C in a humidified environment with 5% CO_2. Prior to the microscopy experiments, MEF cells were grown to approximately 50% confluency in 35 mm glass-bottomed dishes (Ibidi) suitable for optical microscopy. In turn, MEF were treated during 1h with a PBS 10x (pH7.4) 1% DMSO solution containing compounds 1 or 2 at 10 µM (compounds 1 and 2 were previously dissolved in DMSO to a concentration of 1 mM). Fluorescence images were then recorded while maintaining optimal conditions (37°C and 5% CO_2) with an integrated microscope enclosure.

Theoretical details

The optimum structures of the neutral and charged species of **1**, **2** and their **dimers** were determined in CH_2Cl_2 using the SCRF (self-consistent-reaction-field) theory using the PCM (Polarized Continuum Model) approach.[7] All calculations were performed in the framework of the density functional theory (DFT) using the hybrid meta-GGA functional M06-2X[8] together with the 6-31G** basis set,[9, 10] as implemented in the GAUSSIAN09 program.[11] It is well known that this functional give reliable ground electronic state polarization when compared to X-ray structures[12] and also accurate excited states dipole moments for a large variety of push-pull systems.[13] Furthermore, the molecular geometries of the systems under study were calculated with the long-range corrected hybrid functional CAM-B3LYP[14] to check the long-range correction effects on the optical and electronic properties. Interestingly, both M06-2X and CAM-B3LYP functionals give similar trends in the molecular structure description (Figures 1 and 2 in the main text when compared to Figures S1 and S2), evolution of the energy gaps (Figure 6 in the main text when compared to Figures S7), and vibrational characterization (Figures S3-S6) when comparing the two chromophores. Calculations on radical cations were spin-unrestricted. Note that all geometrical parameters were allowed to vary independently apart from planarity of the rings. No imaginary harmonic frequencies were observed, which ensure the finding of the global minimum energy.

Vertical electronic excitation energies were performed by using the Time-Dependent DFT (TDDFT) approach[15-17] on the resulting optimized molecular geometries. Absorption spectra were simulated through convolution of the vertical transition energies and oscillator strengths with Gaussian functions (0.3 eV width at the half-height). In addition, the first excited state of monomer species was fully studied by using TD-DFT approach on the previously obtained ground state molecular geometries.

Furthermore, IR and Raman intensities were calculated by using an adjustment of the theoretical force fields in which the frequencies are uniformly scaled down by a factor of 0.965 for both B3LYP and CAM-B3LYP functionals and by a factor of 0.937 for M06-2X functional, to disentangle experimental misassignments. The theoretical spectra were obtaining by convolution the scaled frequencies and the IR/Raman scattering activities with Gaussian functions (10 cm^{-1} width at the half-height).

For the NLO properties, molecular hyperpolarizabilities at zero frequency were calculated at M06-2X/6-31G** level and the default parameters provided by the "polar" keyword.

Molecular orbital contours and vibrational eigenvector were plotted using the ChemCraft 1.8 molecular modelling software.[18]

2PA properties were calculated at the TD-DFT/CAM-B3LYP level on the minimal ground-state geometries by using Dalton 2018 with default parameters.[19, 20] The 6-31G** basis set was employed and the first ten electronic transitions were examined. 2PA spectra were then simulated with Gaussum from these transitions.[21]

2. Syntheses

Compounds **4** and **5** were prepared as previously described.[22] *p*-diphenylaminobenzaldehyde (**3**) is commercially available.

3-(2,6-bis((*E*)-4-(diphenylamino)styryl)-4*H*-pyran-4-yliden)-2-phenylprop-1-ene-1,1,3-tricarbonitrile (1)

This compound had been already reported.[23] For this article, compound **1** was prepared by following the same procedure as for **2**, starting from **4** (150 mg, 0.5 mmol) and **3** (273 mg, 1 mmol) in 7.5 mL of acetonitrile with 100 μL (1 mmol) of piperidine. The purificaction of the compound was carried out by flash chromatography (silica gel) with CH_2Cl_2/hexane 8.5:1.5 as eluent, to obtain a dark violet solid that is washed with a mixture of pentane/CH_2Cl_2 9:1. Yield: dark violet solid (70.3 mg, 17 %).

In addition to the described characterization, the following data were now incorporated:

Mp: 289-291 °C.

Elemental analysis: C, 84.7; H, 4.65; N 8.8. Calc. $C_{57}H_{39}N_5O$ (C, 84.5; H, 4.85; N 8.65 %).

δH (400 MHz; CD_2Cl_2) 5.90 (1H, br s, CH pyran), 6.38 (1 H, br d, *J* 15.0, HC=), 6.74 (1 H, br d, *J* 15.0, HC=), 6.93 (1 H, br s, CH pyran), 7.00–7.02 (4 H, m, Ar-H), 7.11–7.15 (12 H, m, Ar-H), 7.30–7.46 (12 H, m, Ar-H), 7.53–7.65 (6 H, m, Ar-H).

HRMS (MALDI): m/z 832.3042 [M+Na]+, calc. for $C_{57}H_{39}N_5NaO$ 832.3047.

2-(4-((2,6-bis((*E*)-4-(diphenylamino)styryl)-4*H*-pyran-4-yliden)methyl)-3-cyano-5,5-dimethylfuran-2(5*H*)-yliden)malononitrile (2).

To a solution of 104 mg (0.34 mmol) of compound **5** and 186 mg (0.68 mmol) of *p*-diphenylaminobenzaldehyde (**3**) in acetonitrile (5 mL), piperidine (70 μL, 0.07 mmol) was added. The mixture was heated at reflux under an argon atmosphere with exclusion of light (TLC monitoring) for 9h 20 min. After cooling, the solvent was evaporated, and the crude product was purified by flash chromatography (silica gel) with CH_2Cl_2/hexane 10:2 as eluent, to obtain a dark blue solid that is washed with a mixture of pentane/CH_2Cl_2 8:2. This solid is re-purified by flash chromatography (silica gel) with AcOEt/hexane 2:8 as eluent, then the polarity is increased slowly to AcOEt. Yield: dark blue solid (23.0 mg, 8 %).
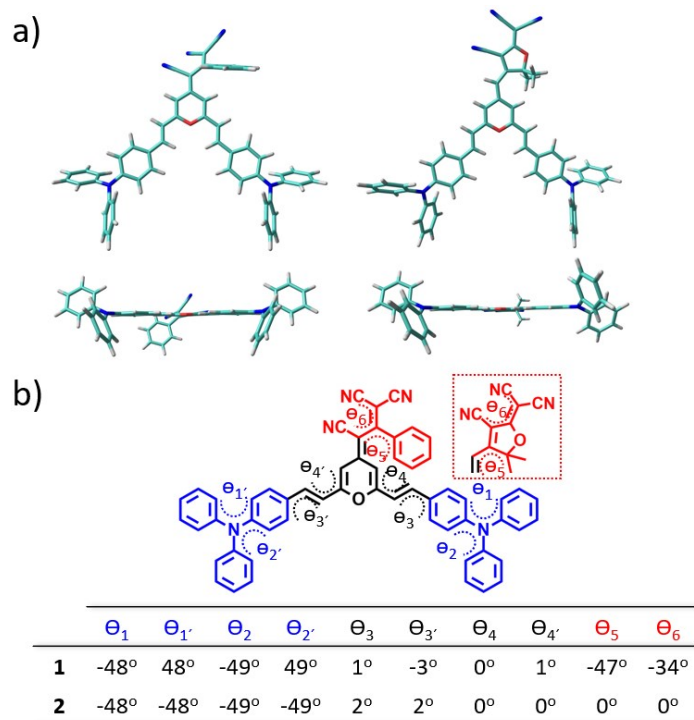
Mp: 296 °C (dec).

Elemental analysis: C, 82.2; H, 5.35; N 8.8. Calc. $C_{56}H_{41}N_5O_2$ (C, 82.4; H, 5.1; N 8.6 %).

δH (400 MHz; CD_2Cl_2) 1.58 (6 H, s, 2×CH3), 6.66–6.77 (5H, m, 2× HC= + 3 Ar-H), 7.00–7.04 (4H, m, Ar-H), 7.11–7.16 (12 H, m, Ar-H), 7.30–7.35 (8 H, m, Ar-H), 7.46–7.50 (m, 4H, Ar-H), 7.55 (2H, d, *J* 16.0, 2× HC=).
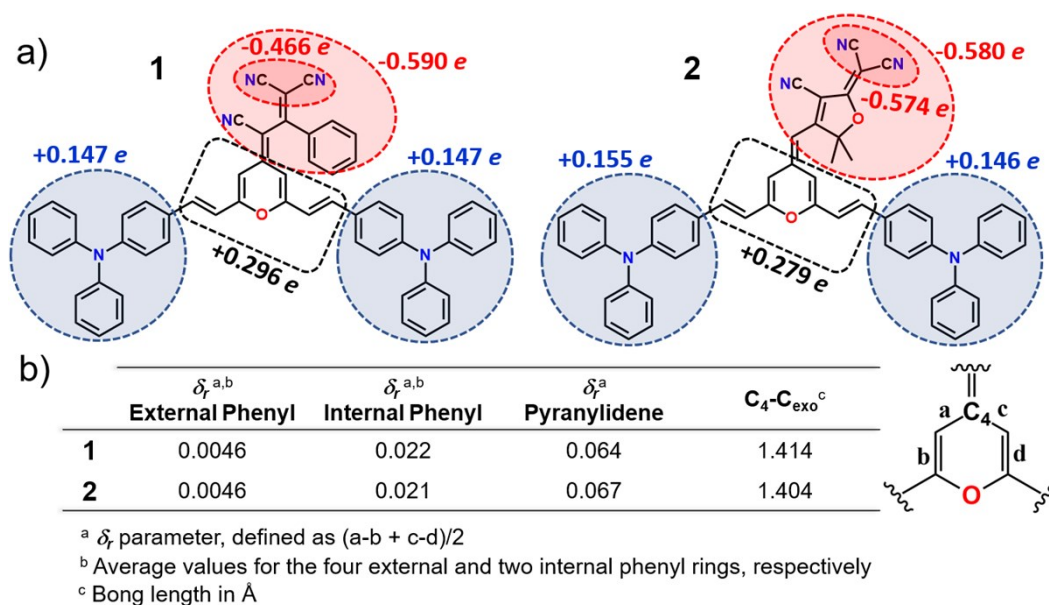
^{13}C NMR: not registered due to its low solubility.

HRMS (MALDI): m/z 838.3110 [M+Na]+, calc. for $C_{56}H_{41}N_5NaO_2$ 838.3152.

## 3. DFT calculations

	Θ_1	$\Theta_{1'}$	Θ_2	$\Theta_{2'}$	Θ_3	$\Theta_{3'}$	Θ_4	$\Theta_{4'}$	Θ_5	Θ_6
1	-48°	48°	-49°	49°	1°	-3°	0°	1°	-47°	-34°
2	-48°	-48°	-49°	-49°	2°	2°	0°	0°	0°	0°

Figure S1. a) Top and lateral views of the DFT-optimized structures for **1** and **2** systems at the PCM-CAM-B3LYP/6-31G** level using CH_2Cl_2 as solvent. b) DFT-calculated inter-ring dihedral angles (θ) along the conjugated backbones of **1** and **2** using the same level of theory.

	δ_r [a,b] External Phenyl	δ_r [a,b] Internal Phenyl	δ_r [a] Pyranylidene	C_4-C_{exo} [c]
1	0.0046	0.022	0.064	1.414
2	0.0046	0.021	0.067	1.404

[a] δ_r parameter, defined as (a-b + c-d)/2
[b] Average values for the four external and two internal phenyl rings, respectively
[c] Bong length in Å

Figure S2. a) Mülliken atomic charges on various molecular domains and b) structural parameters for chromophores **1** and **2** calculated at the PCM-CAM-B3LYP/6-31G** level using CH_2Cl_2 as solvent.
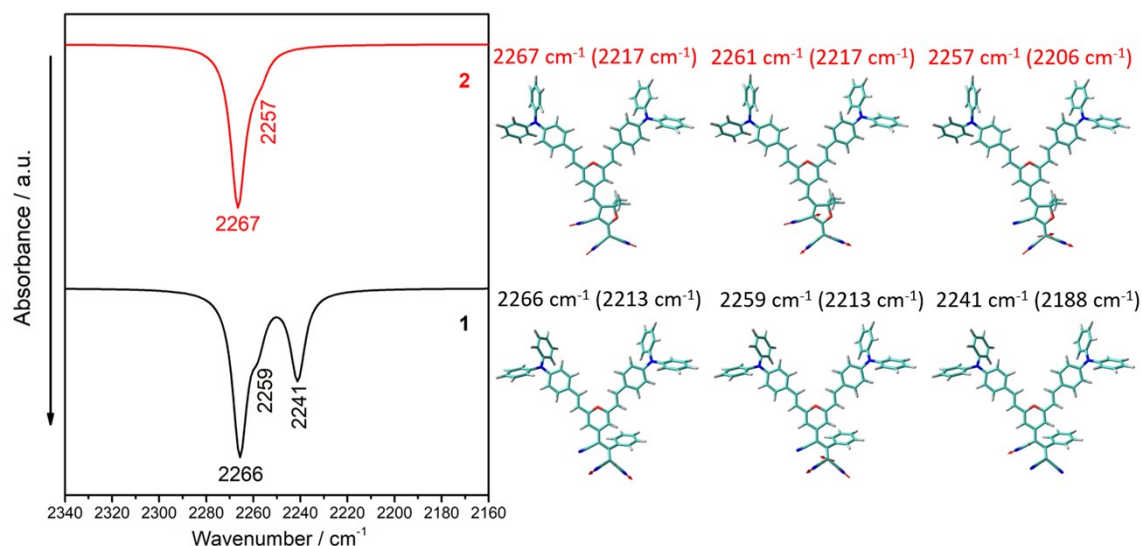
Figure S3. Theoretical IR spectrum and vibrational eigenvectors associated with the ν(C≡N) features for the previously optimized structures of **1** and **2** at M06-2X/6-31G** level. The theoretical and experimental (in parentheses) wavenumbers are also shown.
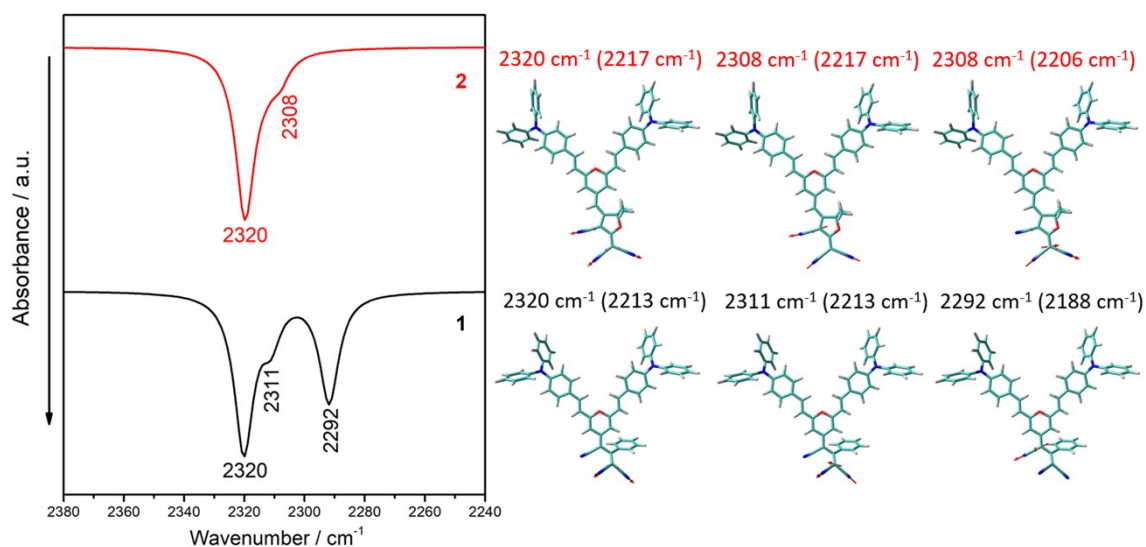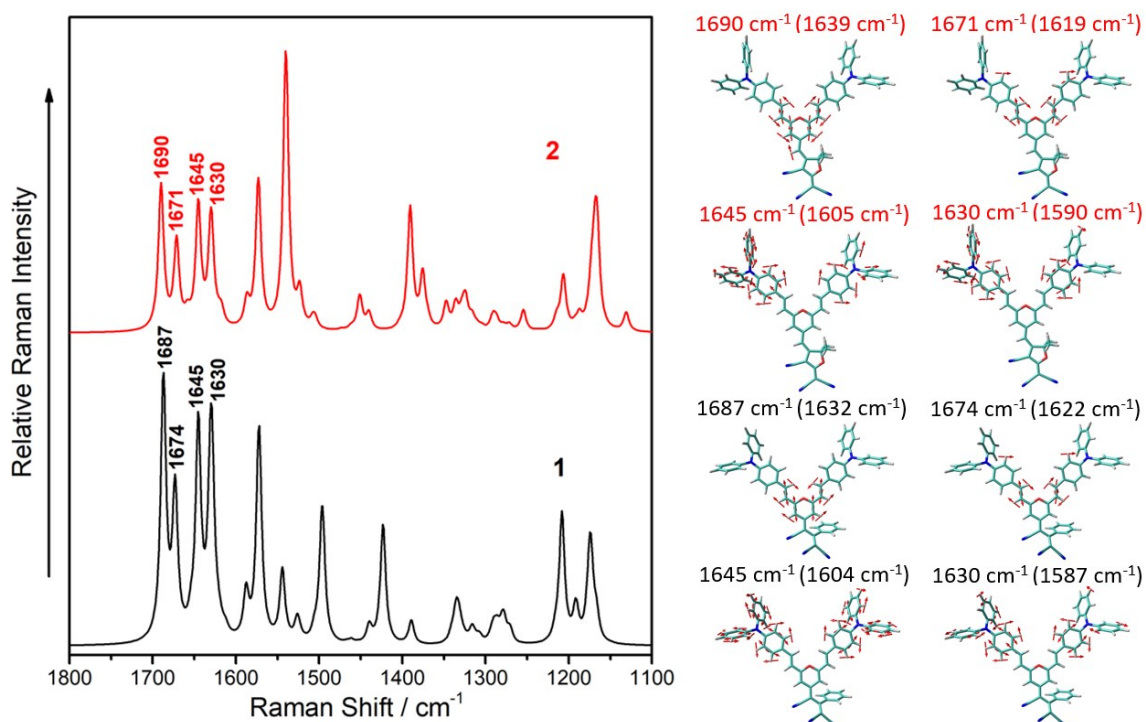

Figure S4. Theoretical IR spectrum and vibrational eigenvectors associated with the ν(C≡N) features for the previously optimized structures of **1** and **2** at CAM-B3LYP/6-31G** level. The theoretical and experimental (in parentheses) wavenumbers are also shown.

S8
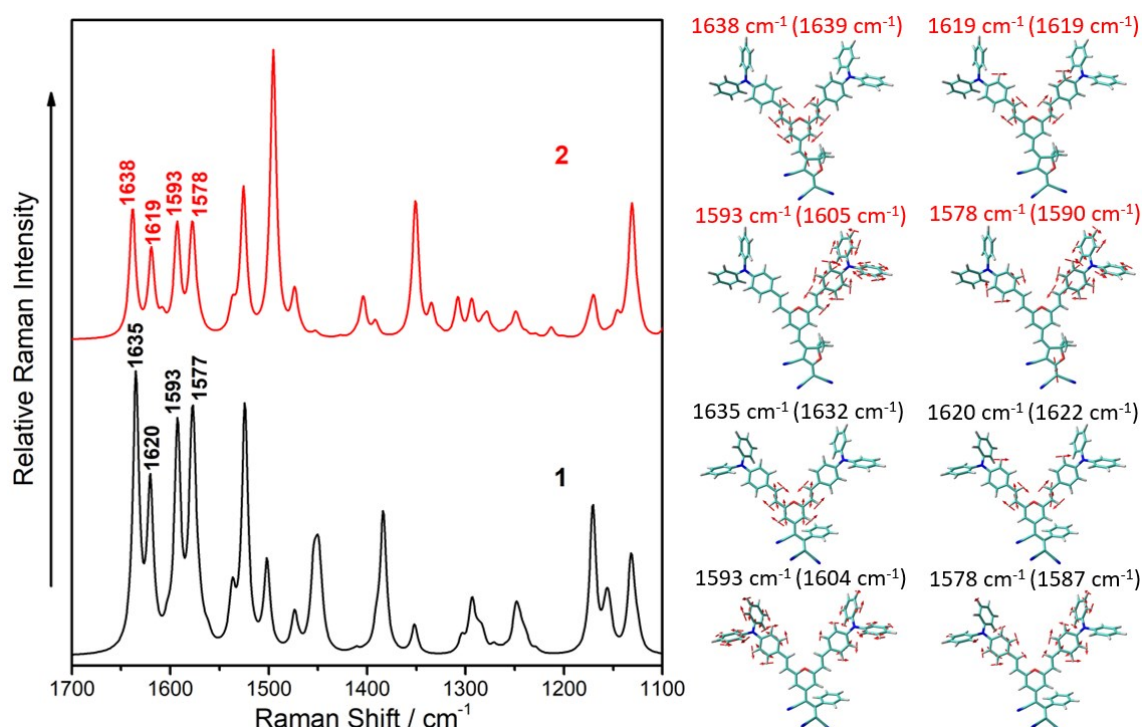
Figure S5. M06-2X/6-31G** Raman spectrum and vibrational eigenvectors associated with the most outstanding C=C/C-C Raman features in the 1640-1590 cm^{-1} region of molecules **1** and **2**. The theoretical and experimental (in parentheses) wavenumbers are also shown.

Figure S6. CAM-B3LYP/6-31G** Raman spectrum and vibrational eigenvectors associated with the most outstanding C=C/C-C Raman features in the 1640-1590 cm^{-1} region of molecules **1** and **2**. The theoretical and experimental (in parentheses) wavenumbers are also shown.

4. Photophysical properties and TD-DFT calculations
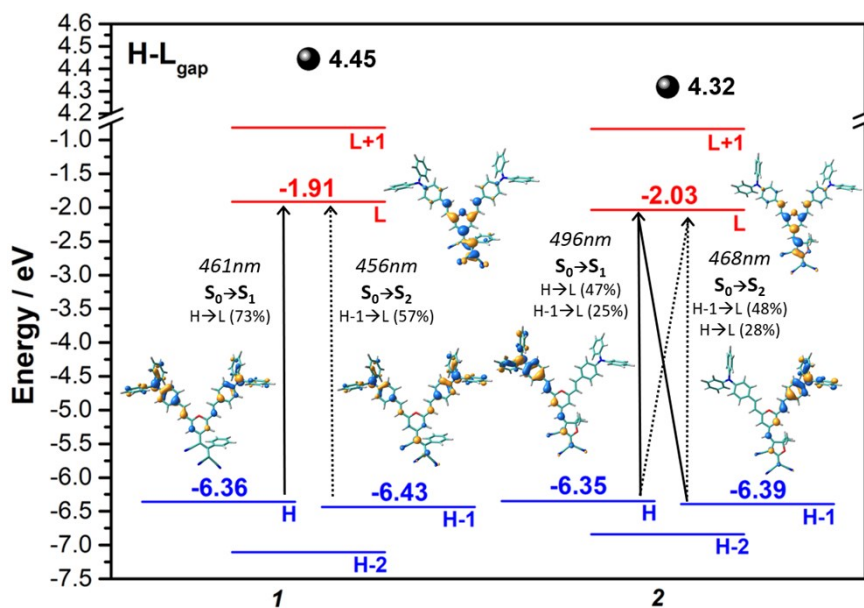
Figure S7. DFT-calculated frontier molecular orbital energies and topologies for **1** and **2**, at the PCM-CAM-B3LYP/6-31G** level using CH_2Cl_2 as solvent. The $S_0 \rightarrow S_1$ and $S_0 \rightarrow S_2$ electronic transitions are also shown as solid and dashed black arrows, respectively.

	M062X		CAM-B3LYP	
	1	**2**	**1**	**2**
θ_1	-44° (-45°)	-45° (-45°)	-48° (-46°)	-48° (-50°)
$\theta_{1'}$	44° (44°)	-45° (-45°)	48° (47°)	-48° (-50°)
θ_2	-46° (-45°)	-46° (-41°)	-49° (-50°)	-49° (-45°)
$\theta_{2'}$	45° (44°)	-46° (-47°)	49° (50°)	-49° (-46°)
θ_3	2° (3°)	5° (6°)	1° (1°)	2° (0°)
$\theta_{3'}$	-3° (1°)	5° (0°)	-3° (-1°)	2° (2°)
θ_4	1° (1°)	1° (2°)	0° (0°)	0° (0°)
$\theta_{4'}$	0° (1°)	1° (0°)	1° (1°)	0° (0°)
θ_5	-45° (-45°)	0° (0°)	-47°(-50°)	0° (0°)
θ_6	-32° (-27°)	0° (0°)	-34° (-26°)	0° (0°)

Dihedral angles values for the ground (first excited) state
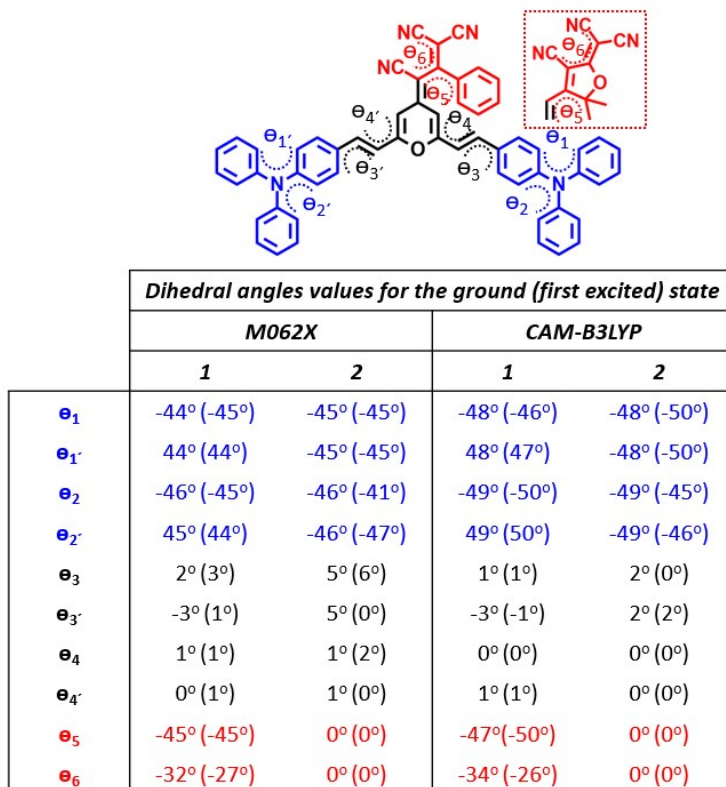
Figure S8. DFT-calculated inter-ring dihedral angles (ɵ) for the ground (first excited) state of **1** and **2** at the PCM-M06-2X/6-31G** and PCM-CAM-B3LYP/6-31G** level of theory using CH_2Cl_2 as solvent.
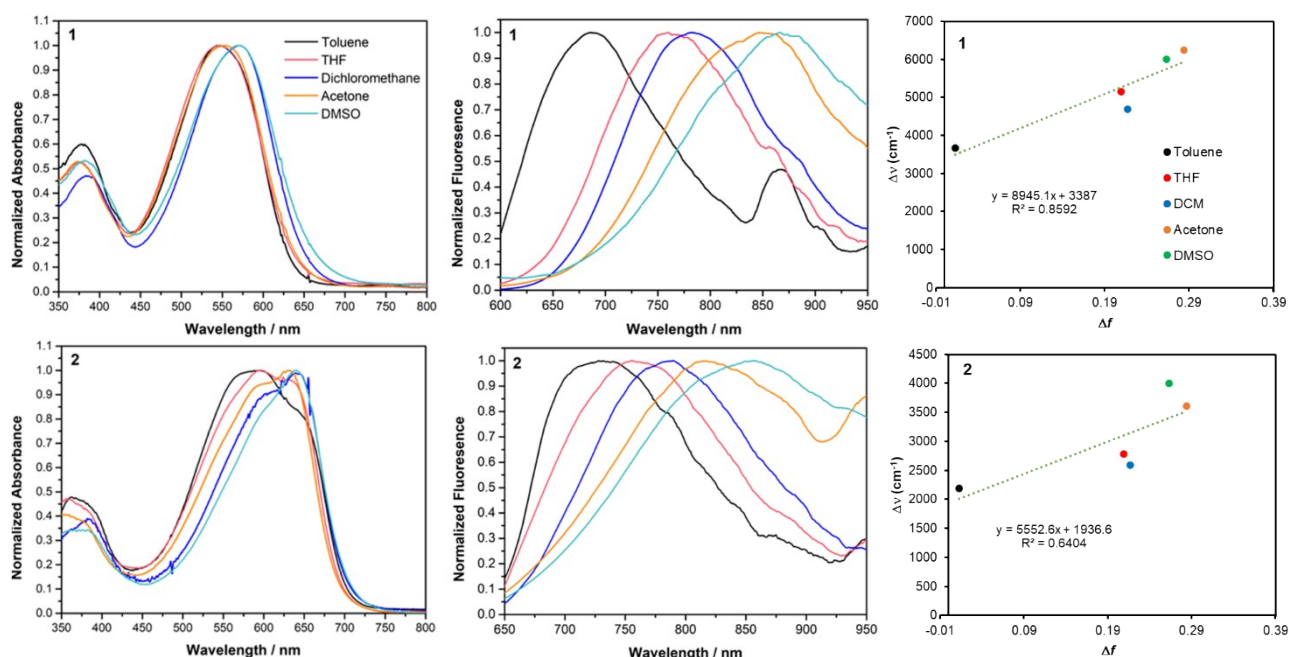
Figure S9. UV-vis absorption (left) and fluorescence spectrum (central) variation for compounds **1** (top) and **2** (bottom) in different solvents. Lippert-Mataga plot is represented as well (right) for both derivatives. From the linear fit data, the dipole moment changes between the excited and the ground states are estimated in 19.6 and 15.2 D respectively. Employed solvents: Toluene (black), Tetrahydrofuran (red), Dichloromethane (blue), Acetone (orange) and DMSO (light green).

Table S1. DFT-Calculated molecular dipole moments for the ground state (μ_g), first (μ_{S1}) and second (μ_{S2}) excited states of compounds **1** and **2**. The calculations have been done at PCM-M06-2X/6-31G** level of theory using CH_2Cl_2 as solvent.

		M06-2X/6-31G**
	μ_g (D)	24.9
1	μ_{s1} (D)	41.2
	μ_{s2} (D)	30.7
	μ_g (D)	31.8
2	μ_{s1} (D)	33.7
	μ_{s2} (D)	51.1
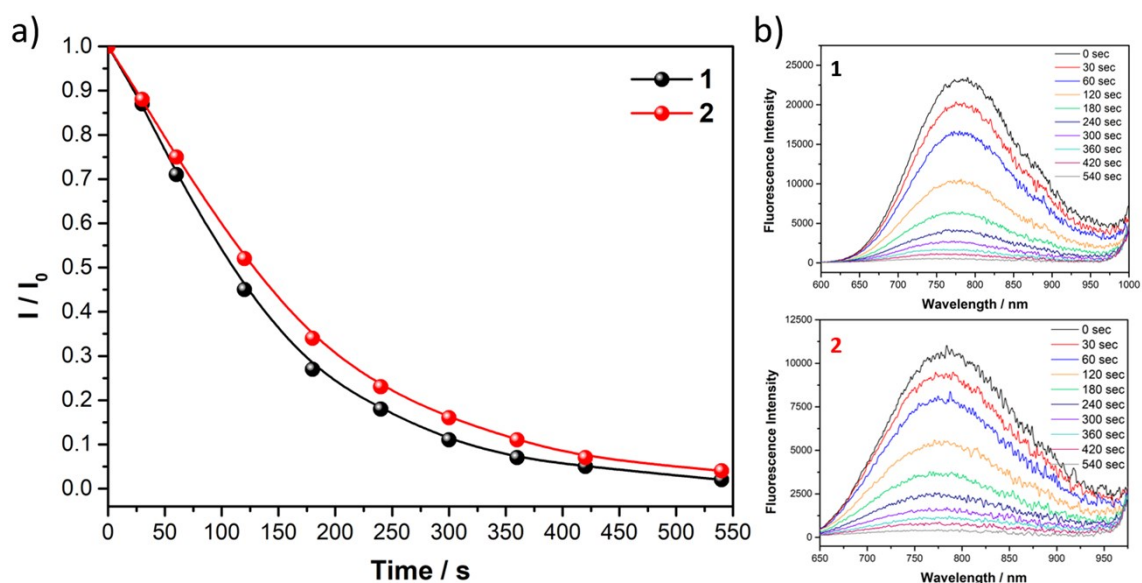
Figure S10. a) Time-dependent fluorescence intensity of compounds **1** (λ_{exc} = 580nm) and **2** (λ_{exc} = 640nm) in CH_2Cl_2 under the irradiation of a 254 nm light in the presence of air. b) The fluorescence intensity was monitored at the band maxima.
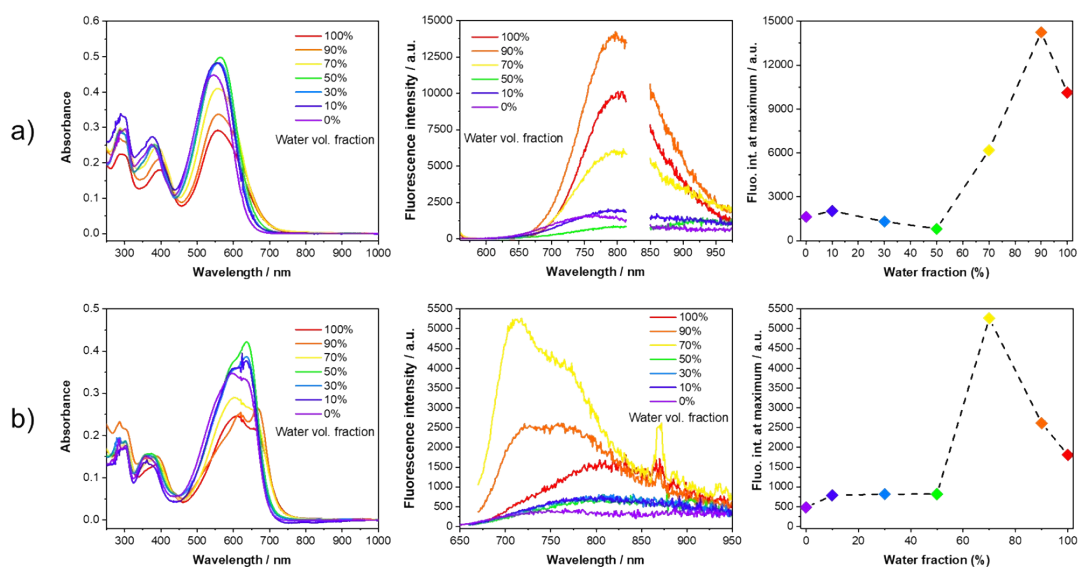
Figure S11. UV-vis absorption (first column) and fluorescence (second column) spectra of compound a) **1** and b) **2** in THF/water mixtures with different water fractions. The dependence of the fluorescence intensity as function of the water volume fraction is represented in the third column.

5. Spectroelectrochemical and electrochemical properties
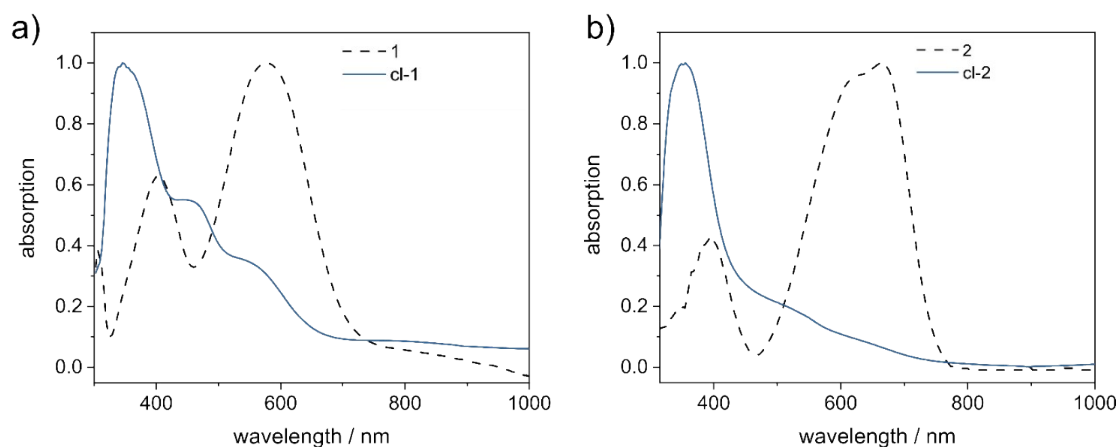
Figure S12. Comparison between the UV-Vis absorption of neutral pure chromophore (dashed line, spin coated) and neutral film after electrochemical deposition for **1** (b) and **2** (b) systems. The spectra of the neutral states (blue) are taken from spectroelectrochemistry experiments previously shown in the main text (see Figures 7e and f of the manuscript).
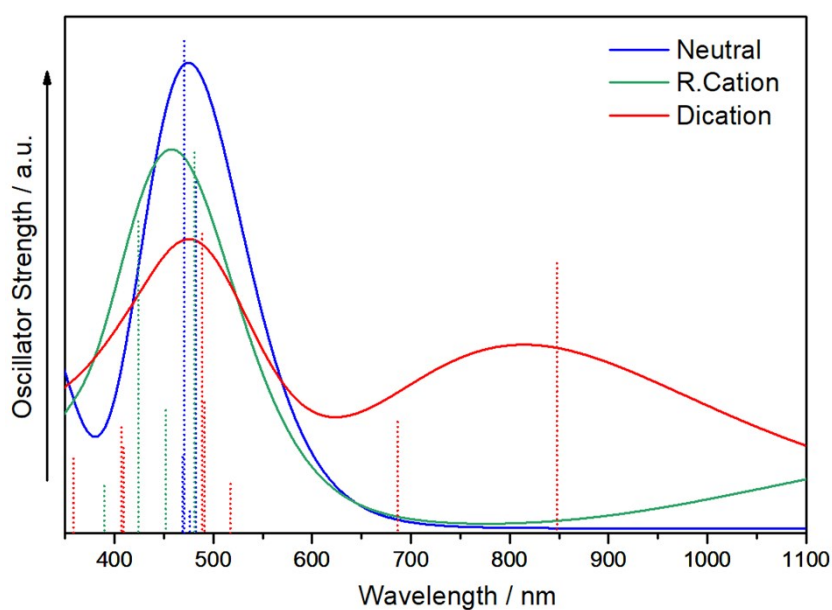
Figure S13. Simulated absorption spectra and main excitations (oscillator strength vs. wavelength) shown as vertical bars for neutral, radical cation and dication states of chromophore **1** dimers as determined with TD-DFT at the PCM-M06-2X/6-31G** level using CH_2Cl_2 as solvent.

Discussion about chemical doping:

An alternative technique to initiate oxidative coupling reactions between the chromophores is simultaneous doping and polymerization by chemical doping.[24] Our approach included the strong oxidative dopant $FeCl_3$ which was brought into contact with the chromophore film through the vapor phase. For the chemical doping approach films of pure chromophores were spin coated and afterwards exposed to $FeCl_3$ vapor. The doping process was followed in-situ by UV-vis spectroscopy, Figure S14. Afterwards, the simultaneously doped and polymerized films were further characterized in the electrochemical setup to enable comparison to the electrochemically polymerized films (see Figure S15 and S16).

As doping proceeds, both charge transfer bands of the chromophores, located around 600 nm decrease in favor of new signals below 380 nm and above 800 nm. The transition of one electronic species into the other is emphasized by the existence of two distinct isosbestic points at around 500 nm and 700 nm. Since the developing bands at 380 nm and above 800 nm certainly differ from the observed signals from the electrochemically polymerized films (see Table S2) we tend to assign these bands to mostly uncoupled but charged monomeric species of the two chromophores. The assigned characteristic absorption bands are summarized in Table S2.

Although not entirely polymerized the chemically doped chromophore films still contain a certain amount of TPB units making the films insoluble in acetonitrile and allowing for a subsequent spectroelectrochemical characterization (see Figures 15 and 16). Besides previously discussed characteristic bands of TPB dimeric species more pronounced monomeric bands can be observed at 576 nm (**1**) and 663 nm (**2**). Comparing the data to the electrochemically polymerized films, the amount of isolated chromophores seems to be higher in the chemically doped and polymerized films.
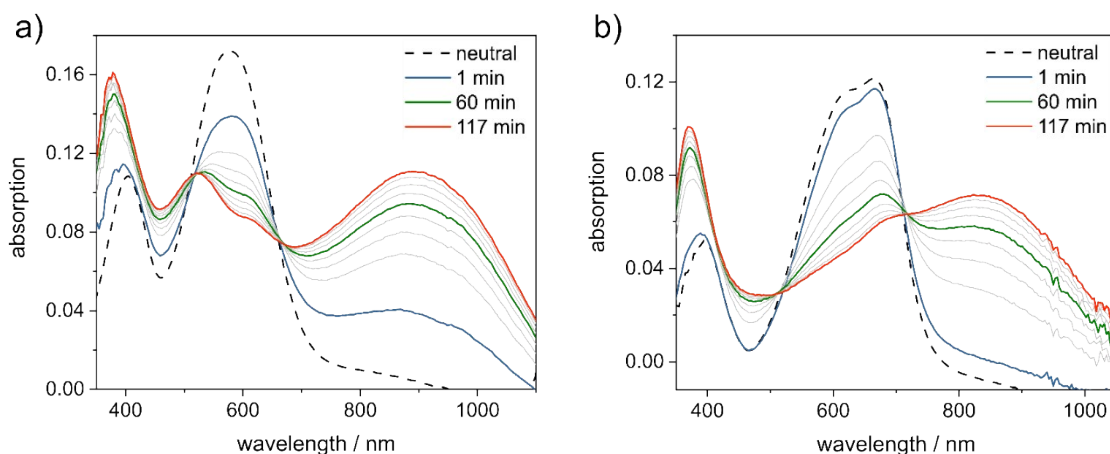
Figure S14. *In-situ* UV-Vis data of simultaneous doping and polymerization through vapor phase of films of **1** in a) and of **2** in b) with $FeCl_3$ at reduced pressures of $2.6 \cdot 10^{-2}$ mbar. The black dashed lines represent the neutral chromophore films at the beginning before vapor doping.
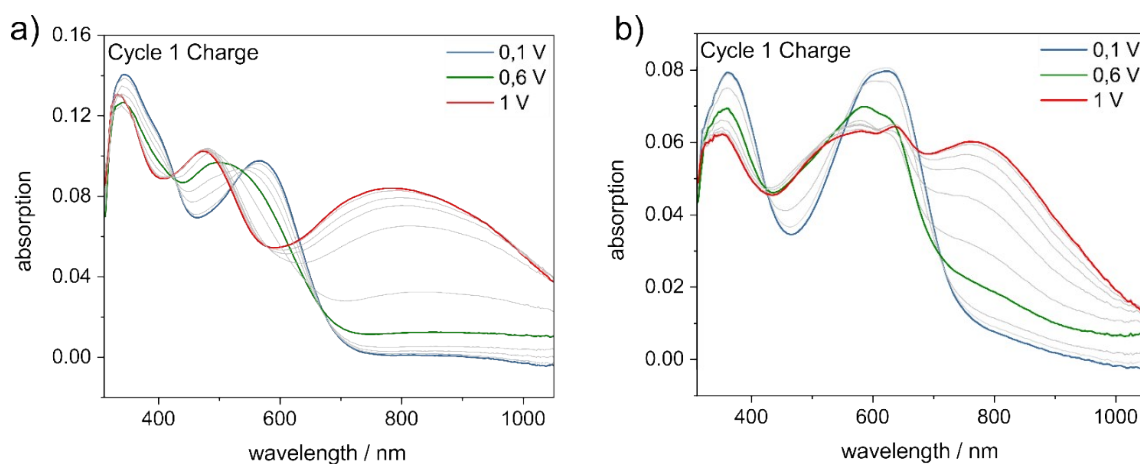
Figure S15. Absorption behavior during first cycles of in-situ spectroelectrochemistry of chemically doped and polymerized films on ITO substrates in monomer free solution (0.1 M TBAPF$_6$ in MeCN, 20 mVs^{-1}) of cl-**1** (a) and cl-**2** (b) as prepared according to Figure S14.
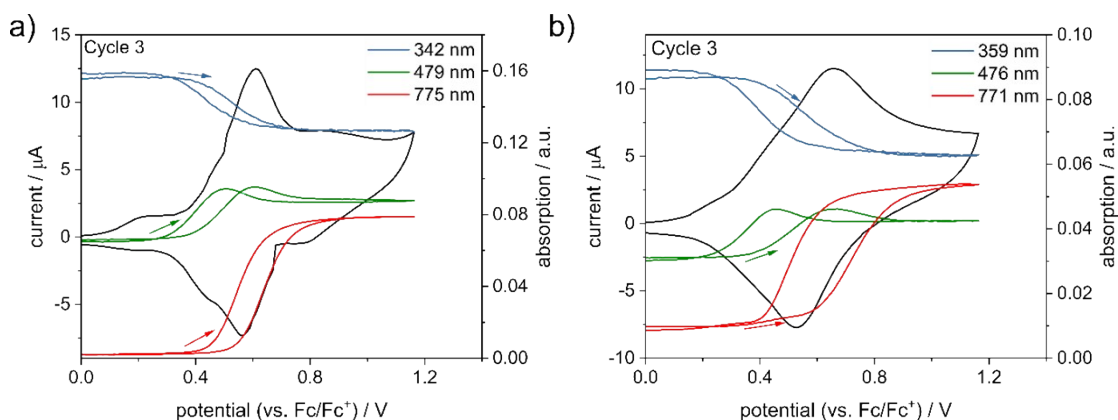

Figure S16. In-situ spectroelectrochemistry of chemically doped and polymerized films on ITO substrates in monomer free solution (0.1 M TBAPF$_6$ in MeCN, 20 mVs^{-1}) of cl-**1** (a) and cl-**2** (b) during third cycles as prepared according to Figure S15. The respective corresponding evolutions of characteristic absorption bands are given as function of potential.

Table S2. Characteristic absorption bands for chemically doped and polymerized films of **1** and **2**.

	$\lambda_{neutral}$ (nm)	$\lambda^*_{charged}$ (nm)
1	403, 576	380, 525, 892
2	394, 626 (shoulder), 663	372, 835

* can be a radical cation and/or a dication

6. Nonlinear Optical properties
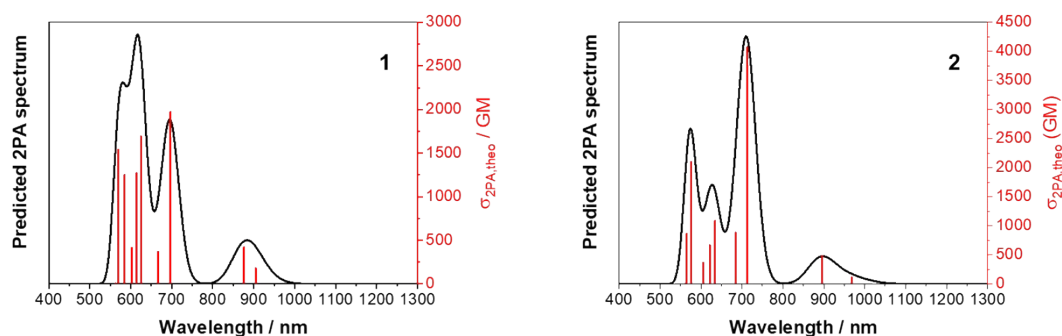
Figure S17. Simulated 2PA spectra (black lines) for compound **1** (left) and **2** (right) at CAM-B3LYP/6-31G** level of theory. As red lines, the predicted intensities of the first ten electronic transitions under 2P regime are indicated.
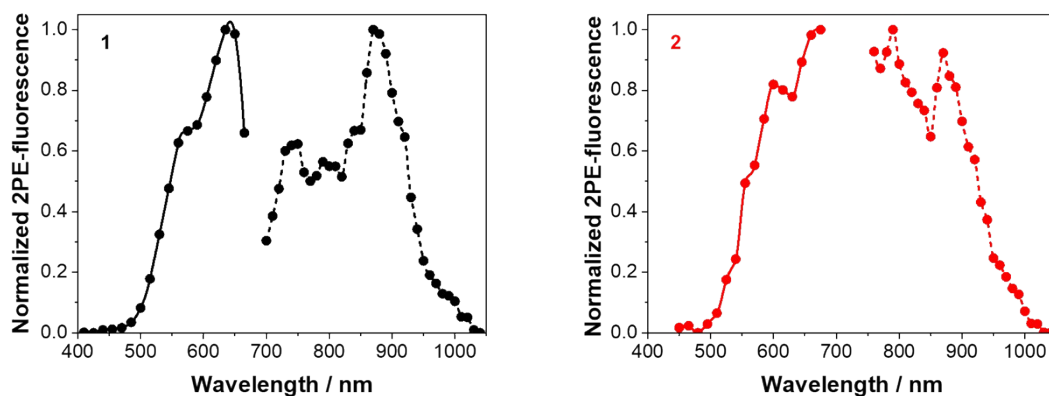
Figure S18. Two-photon excitation (dashed lines) and two-photon excited emission (solid lines) spectra of 10 µM solution of compounds **1** (left) and **2** (right) in aerated toluene.
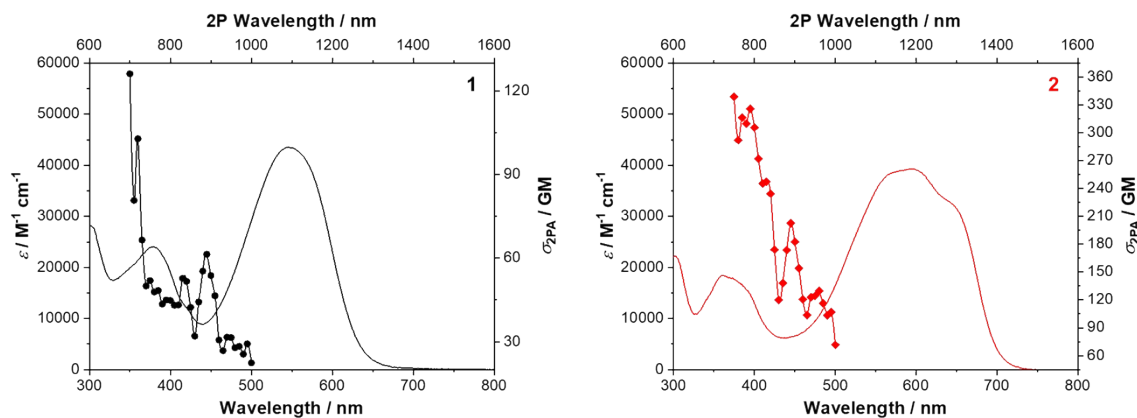

Figure S19. Comparison between the 1PA (solid line) and the 2PA (dotted line) spectra for compounds **1** (left) and **2** (right) in toluene (10 µM aerated solutions).
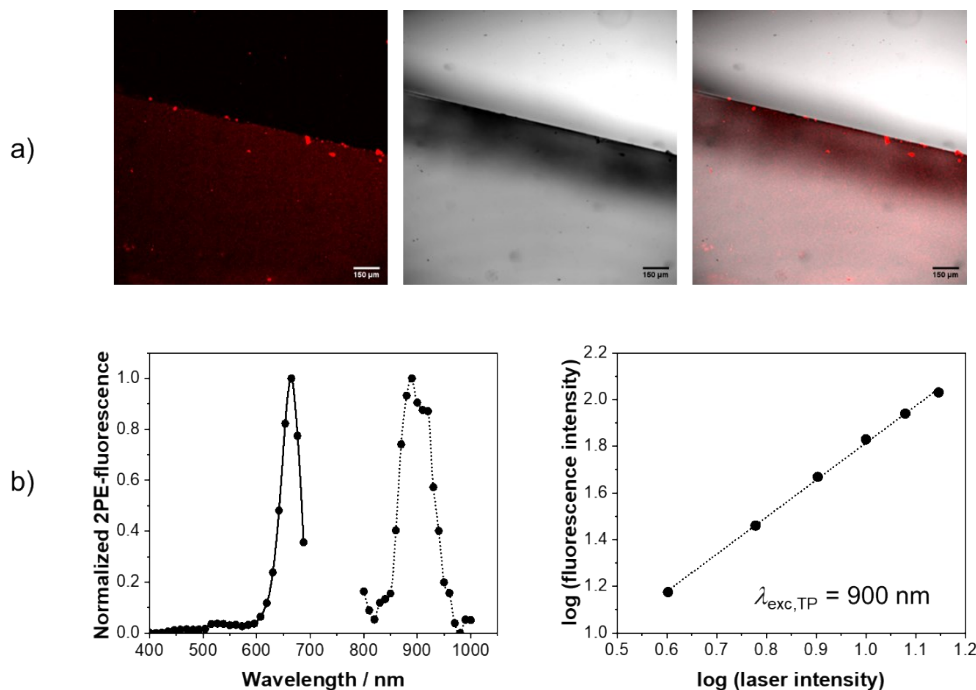
Figure S20. a) 2P-fluorescence imaging of electropolymerized compound **1** (cl-**1**). From left to right: fluorescence image, brightfield image and merge of fluorescence/brightfield images. Scale bar: 150 µm. b) 2P excitation (dashed line) and excited emission (solid line) of cl-**1**. The dependence of the two-photon excited fluorescence intensity on the laser power (slope: 1.6, r^2 = 0.9988) is shown at the right.
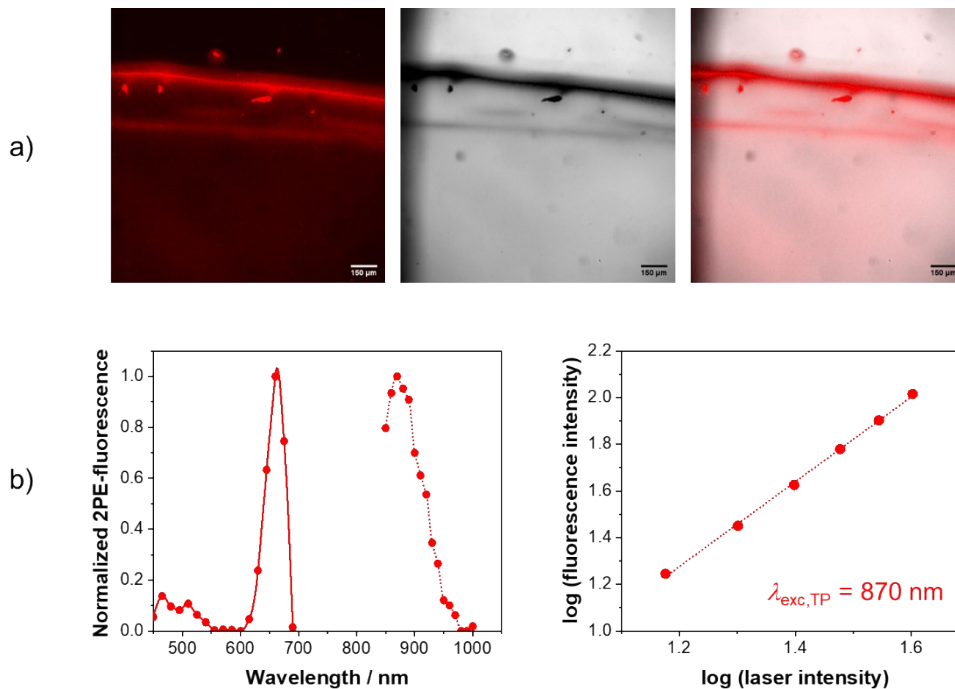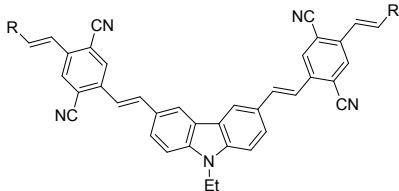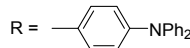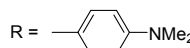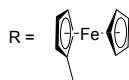

Figure S21. a) 2P-fluorescence imaging of electropolymerized compound **2** (cl-**2**). From left to right: fluorescence image, brightfield image and merge of fluorescence/brightfield images. Scale bar: 150 µm. b) 2P excitation (dashed line with circles) and excited emission (solid line with circles) of cl-**2**. The dependence of the two-photon excited fluorescence intensity on the laser power (slope: 1.8, r^2 = 0.9990) is shown at the right.
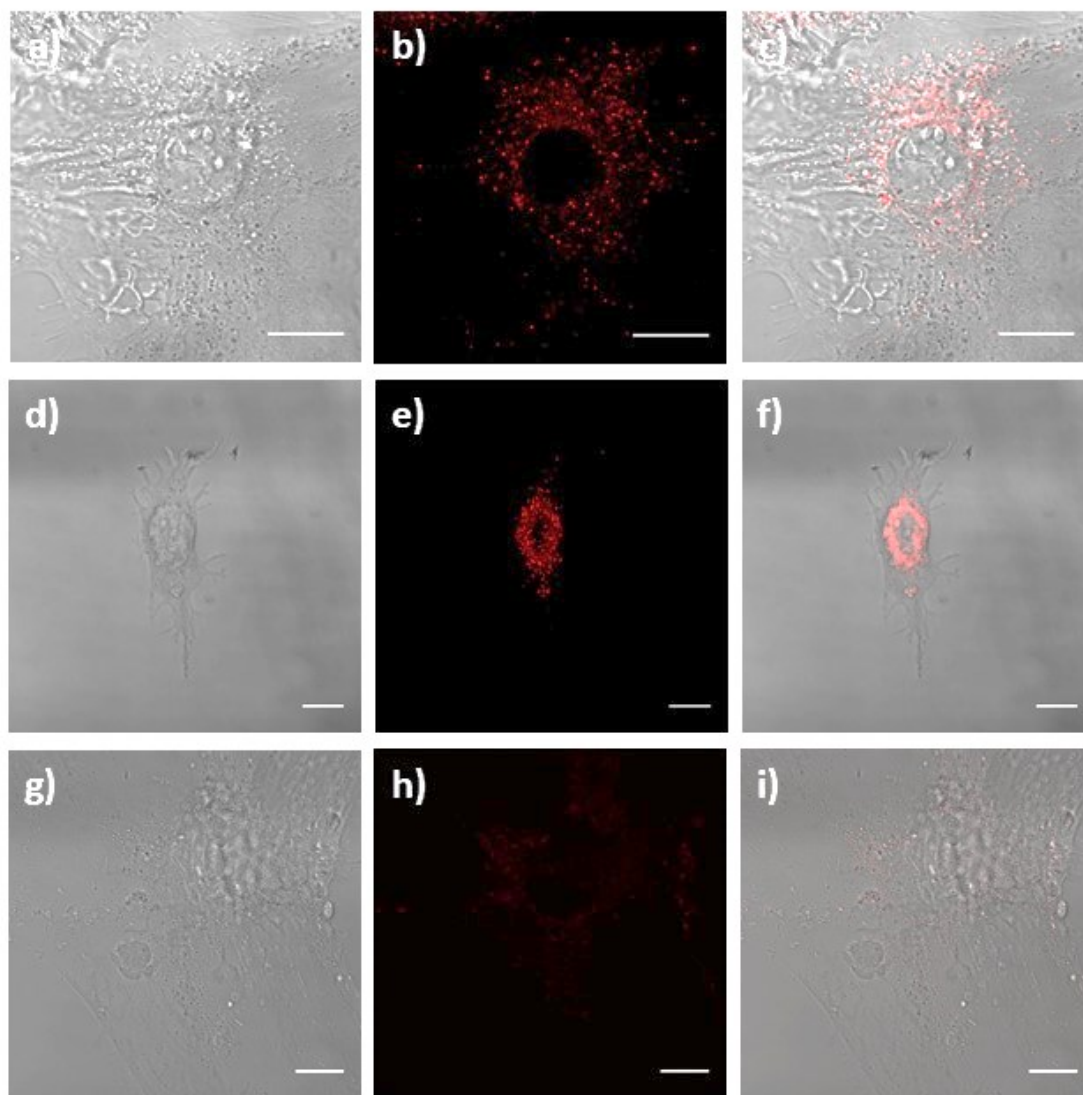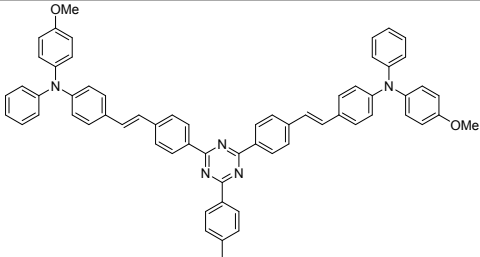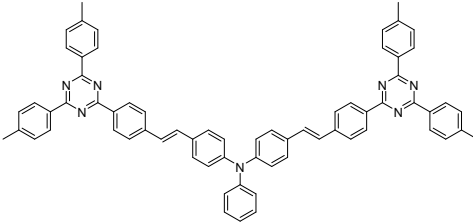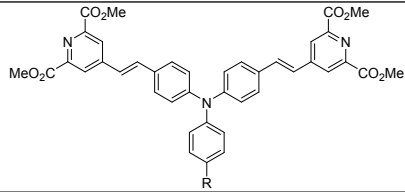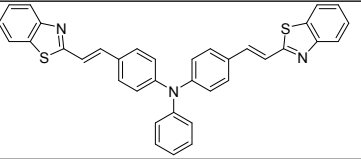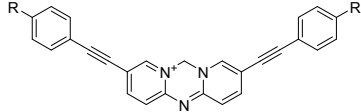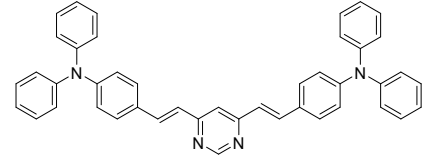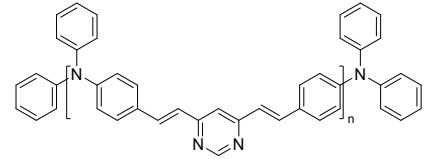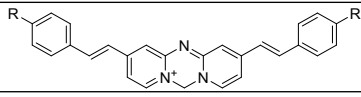
Figure S22. In vivo fluorescence images of dyes **1** (a-c) and **2** (d-f) within MEF cells. Negative control images are also shown in row (g-i). Scale bars: 15 μM.
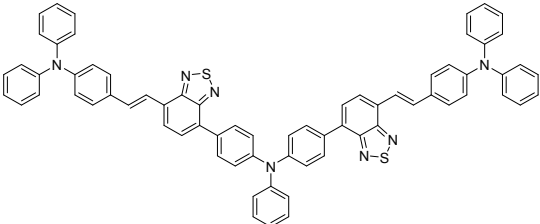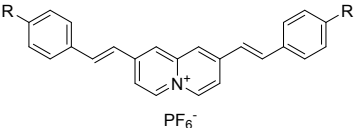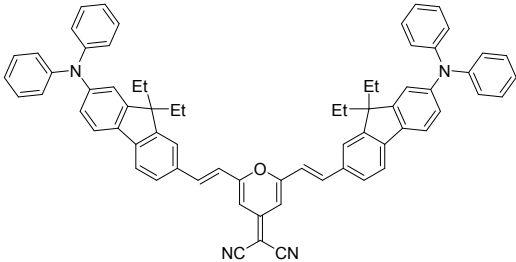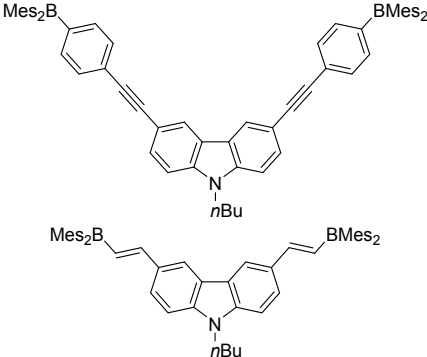
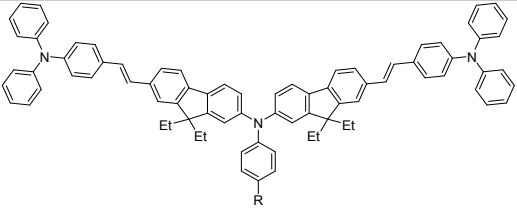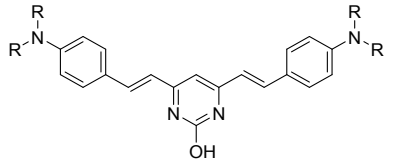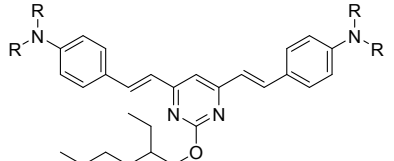## 7. Benchmark of V-shaped molecules with 2PA properties
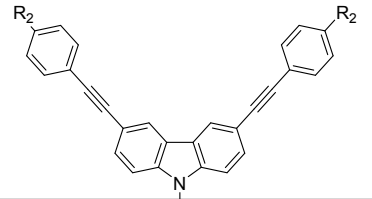
The advantages of the two-photon microscopy have aroused the interest of researchers into development of V-shaped molecules with 2PA properties. As they are not very numerous, the following table shows most of this type of compounds developed for these purpose. Although our compounds do not have the best fluorescence quantum yields, they can be used in fluorescence microscopy, under standard conditions, with promising biological properties.

Table S3. Benchmark of V-shaped molecules with 2PA properties.

Compound		solvent	λ_{abs} [a] (nm)	λ_{em} [b] (nm)	Stokes Shift [c] (nm)	Φ [d]	σ_{2PA} (GM) / [λ_{max} (nm)] [e]	$\Phi\sigma_{2PA}$ (GM)	Reference
	R = —⬡—NPh₂	THF	465	567	102	0.83	3014 [890] [f]	2502	25
		CH₂Cl₂	468	569	101	0.34	2779 [f]	945	
	R = —⬡—NMe₂	THF	458	565	107	0.38	1624 [870] [f]	617	
		CH₂Cl₂	460	570	110	0.21	1413 [f]	297	
	R = Fe	THF	436	558	122	0.004	1515 [830] [g]	6	
		CH₂Cl₂	432	562	130	0.003	1307 [830] [g]	4	
		CHCl₃	423	553	130	--	90 [800] [g]	--	26

Structure	R	Solvent	λ	λ	Δ	Φ	σ	value	Ref
		CHCl$_3$	431	530	99	--	203 [800][g]	--	
	R = H	THF	424	522	98	0.528	208 [800][g]	110	27
	R = CHO	THF	398	483	85	0.617	1380 [800][g]	852	
		EtAcO	422	502	80	0.88	1738 [780][f]	1529	28
	R = NMe$_2$	CH$_2$Cl$_2$	510	616	106	0.01	47 [740][f]	0.5	29
	R = OMe	CH$_2$Cl$_2$	482	525	43	0.26	4200 [740][f]	1092	
		CH$_2$Cl$_2$	431	554	123	0.82	360 [800][f]	295	30
		CH$_2$Cl$_2$	449	558	109	0.63	5093 [800][f]	3209	
	R = OMe	CHCl$_3$	477	507	30	0.19	470 [740][f]	89	31

	R = NMe$_2$	CHCl$_3$	526	596	70	0.25	360 [1050] / 2400 [890] [f]	90		
		Toluene	494	601	107	--	< 1 [900] [f]	--	32	
	R = OMe	MeOH	432	546	114	0.22	1144 [740] [f]	252	33	
	R = NMe$_2$	MeOH	518	650	132	0.003	341 [740] [f]	1		
		CHCl$_3$	488	678	190	0.32	1700 [800] [f]	544	34	
		Toluene	385	466	81	0.89	350 [770] [f]	312	35	
		Toluene	410	431	21	0.04	< 50 [820] [f]	< 2		

Structure	R	Solvent	Abs	Em	Stokes	Φ	σ [λ]	value	Ref
	R = COMe	Toluene	308/402	447/472		0.35	397 [730][f]	139	36
	R = H	Toluene	309/407	452/479		0.42	506 [730][f]	213	
	R = Et	CHCl$_3$	491	585	94	0.30	1531 [850]/1689 [920][f]	459 / 507	37
		THF	449	550	101	0.27	647 [820][f]	175	
	R = Ph	CHCl$_3$	480	595	115	0.39	1279 [850]/1670 [930][f]	499 / 651	
		THF	436	536	100	0.33	679 [820][f]	224	
	R = Et	CHCl$_3$	435	515	80	0.45	382 [820][f]	172	
		THF	431	516	85	0.46	350 [800][f]	161	
	R = Ph	CHCl$_3$	432	521	89	0.67	443 [810][f]	297	
		THF	430	524	94	0.75	369 [800][f]	277	
	R$_1$ = C$_5$H$_{11}$ R$_2$ = CHO	CHCl$_3$	383	468	85	0.63	337 [730][a]	212	38
	R$_1$ = CH$_2$Ph R$_2$ = CHO	CHCl$_3$	378	460	82	0.66	308 [730][a]	203	
	R$_1$ = C$_5$H$_{11}$ R$_2$ = NO$_2$	THF	390	546	156	0.065	645 [770][f]	42	

			[a]	[b]	[c]	[d]	[e]	[g]	
	R$_1$ = CH$_2$Ph R$_2$ = NO$_2$	THF	384	544	160	0.065	916 [780] [f]	60	
This work	**Compound 1**	**Toluene**	**545**	**665**	**120**	**0.009**	**103 [720] /53 [830]** [f]	**0.9 / 0.5**	**This work**
	Compound 2	**Toluene**	**594**	**735**	**141**	**0.002**	**326 [790] / 203 [890]** [f]	**0.7 / 0.4**	

[a] Longest wavelength absorption maximum. [b] Fluorescence emission maximum. [c] The Stokes shift, which is given by the difference between the maxima and emission spectra. [d] Fluorescence emission quantum yield. [e] Wavelength corresponding to the highest cross section. [f] Determined by two-photon-excited fluorescence method. [g] Determined by the open aperture Z-scan method.
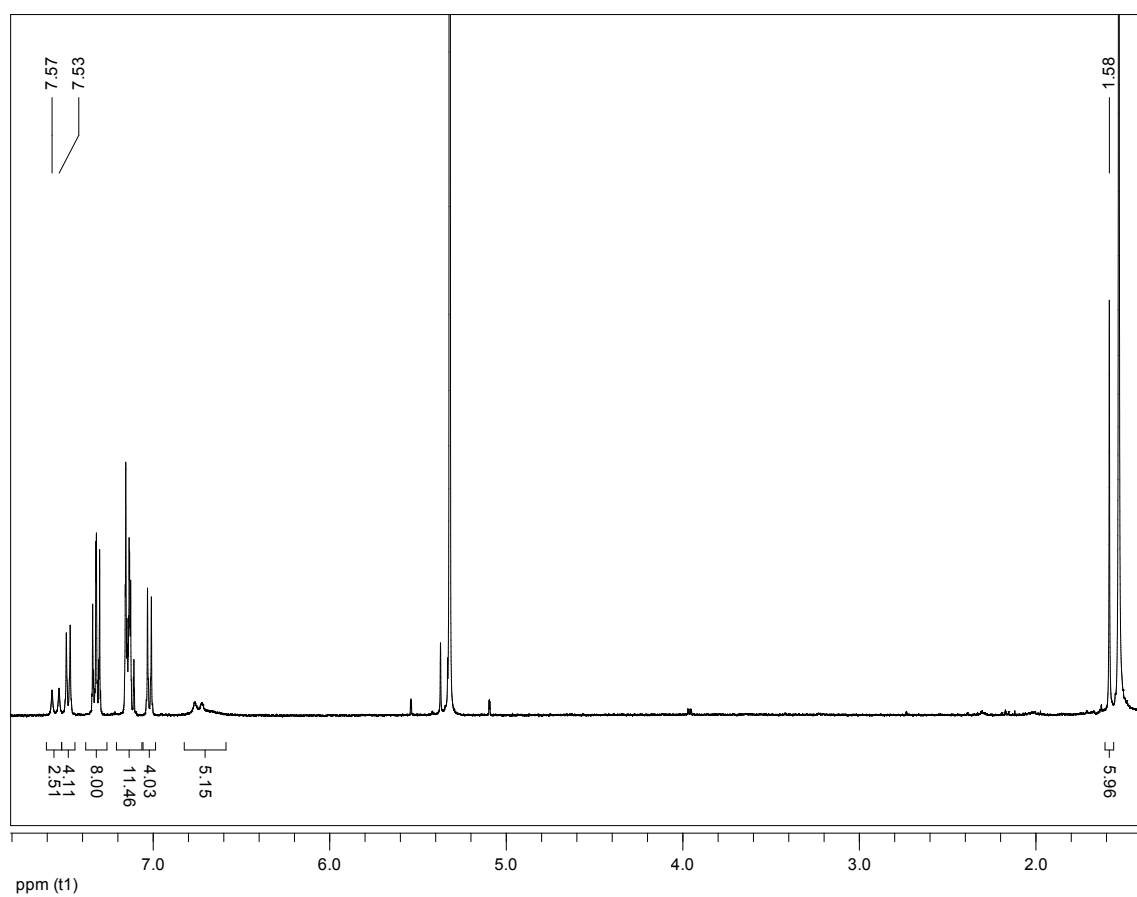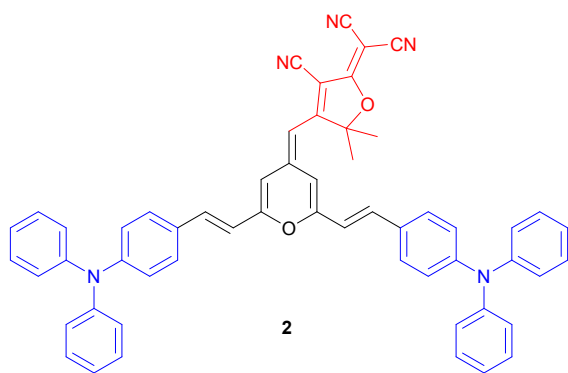
8. ¹H-NMR spectra
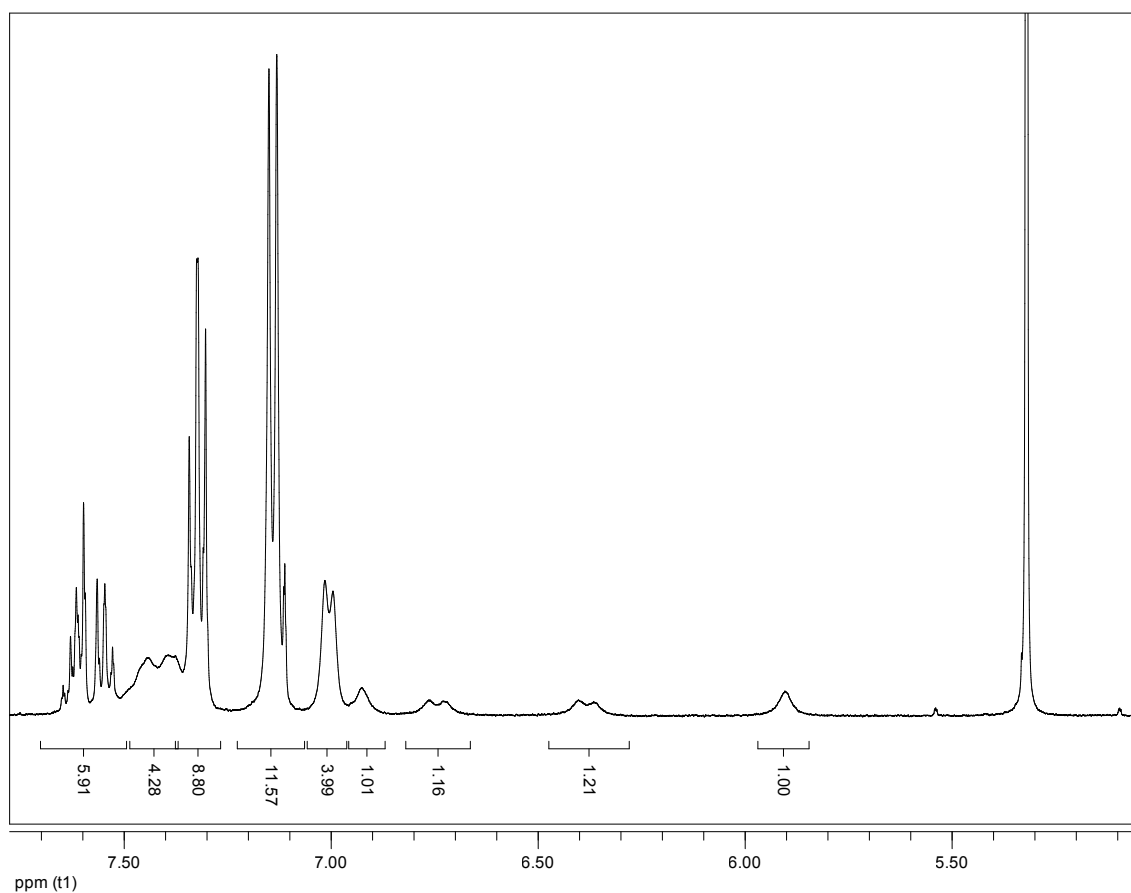
Figure S23: ¹H NMR spectrum of compound **1** (400 MHz, CD₂Cl₂).
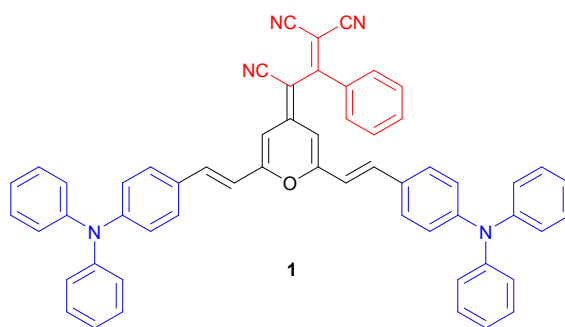
Figure S24: ^{1}H NMR spectrum of compound **2** (400 MHz, CD$_2$Cl$_2$).

2

9. Supporting References

1. J. L. Oudar and D. S. Chemla, *The Journal of Chemical Physics*, 1977, **66**, 2664-2668.
2. C. W. Dirk, H. E. Katz, M. L. Schilling and L. A. King, *Chemistry of Materials*, 1990, **2**, 700-705.
3. A. M. Brouwer, *Pure and Applied Chemistry*, 2011, **83**, 2213-2228.
4. F. Terenziani, C. Katan, E. Badaeva, S. Tretiak and M. Blanchard-Desce, *Advanced Materials*, 2008, **20**, 4641-4678.
5. M. Rumi and J. W. Perry, *Adv. Opt. Photon.*, 2010, **2**, 451-518.
6. L. Qiu, W. S. Lai, D. J. Stumpo and P. J. Blackshear, *Bio-protocol*, 2016, **6**, e1859.
7. J. Tomasi and M. Persico, *Chemical Reviews*, 1994, **94**, 2027-2094.
8. Y. Zhao and D. G. Truhlar, *Accounts of Chemical Research*, 2008, **41**, 157-167.
9. W. J. Hehre, R. Ditchfield and J. A. Pople, *The Journal of Chemical Physics*, 1972, **56**, 2257-2261.
10. M. M. Francl, W. J. Pietro, W. J. Hehre, J. S. Binkley, M. S. Gordon, D. J. DeFrees and J. A. Pople, *The Journal of Chemical Physics*, 1982, **77**, 3654-3665.
11. M. J. Frisch, Trucks, G.W., Schlegel, H.B., et al. , *Wallingford*, 2009

12. C. Moreno-Yruela, J. Garín, J. Orduna, S. Franco, E. Quintero, J. T. López Navarrete, B. E. Diosdado, B. Villacampa, J. Casado and R. Andreu, *The Journal of Organic Chemistry*, 2015, **80**, 12115-12128.
13. F. Castet and B. Champagne, *Journal of Chemical Theory and Computation*, 2012, **8**, 2044-2052.
14. T. Yanai, D. P. Tew and N. C. Handy, *Chemical Physics Letters*, 2004, **393**, 51-57.
15. E. Runge and E. K. U. Gross, *Physical Review Letters*, 1984, **52**, 997-1000.
16. E. K. U. Gross and W. Kohn, in *Advances in Quantum Chemistry*, ed. P.-O. Löwdin, Academic Press, 1990, vol. 21, pp. 255-291.
17. H. H. Heinze, A. Görling and N. Rösch, *The Journal of Chemical Physics*, 2000, **113**, 2088-2099.
18. https://www.chemcraftprog.com,
.
19. K. Aidas, C. Angeli, K. L. Bak, V. Bakken, R. Bast, L. Boman, O. Christiansen, R. Cimiraglia, S. Coriani, P. Dahle, E. K. Dalskov, U. Ekström, T. Enevoldsen, J. J. Eriksen, P. Ettenhuber, B. Fernández, L. Ferrighi, H. Fliegl, L. Frediani, K. Hald, A. Halkier, C. Hättig, H. Heiberg, T. Helgaker, A. C. Hennum, H. Hettema, E. Hjertenæs, S. Høst, I.-M. Høyvik, M. F. Iozzi, B. Jansík, H. J. A. Jensen, D. Jonsson, P. Jørgensen, J. Kauczor, S. Kirpekar, T. Kjærgaard, W. Klopper, S. Knecht, R. Kobayashi, H. Koch, J. Kongsted, A. Krapp, K. Kristensen, A. Ligabue, O. B. Lutnæs, J. I. Melo, K. V. Mikkelsen, R. H. Myhre, C. Neiss, C. B. Nielsen, P. Norman, J. Olsen, J. M. H. Olsen, A. Osted, M. J. Packer, F. Pawlowski, T. B. Pedersen, P. F. Provasi, S. Reine, Z. Rinkevicius, T. A. Ruden, K. Ruud, V. V. Rybkin, P. Sałek, C. C. M. Samson, A. S. de Merás, T. Saue, S. P. A. Sauer, B. Schimmelpfennig, K. Sneskov, A. H. Steindal, K. O. Sylvester-Hvid, P. R. Taylor, A. M. Teale, E. I. Tellgren, D. P. Tew, A. J. Thorvaldsen, L. Thøgersen, O. Vahtras, M. A. Watson, D. J. D. Wilson, M. Ziolkowski and H. Ågren, *WIREs Computational Molecular Science*, 2014, **4**, 269-284.

20. *Dalton a molecular electronic structure program, see* http://daltonprogram.org, Release v2018.2 (2018).
21. N. M. O'boyle, A. L. Tenderholt and K. M. Langner, *Journal of Computational Chemistry*, 2008, **29**, 839-845.
22. R. Andreu, L. Carrasquer, J. Garín, M. J. Modrego, J. Orduna, R. Alicante, B. Villacampa and M. Allain, *Tetrahedron Letters*, 2009, **50**, 2920-2924.
23. X. Wang, Z. Guo, S. Zhu, Y. Liu, P. Shi, H. Tian and W.-H. Zhu, *Journal of Materials Chemistry B*, 2016, **4**, 4683-4689.
24. P. Reinold, K. Bruchlos and S. Ludwigs, *Polymer Chemistry*, 2017, **8**, 7351-7359.
25. Z.-B. Cai, S.-S. Liu, B. Li, Q.-J. Dong, Z.-L. Liu, M. Zheng, S.-L. Li, Y.-P. Tian, L.-J. Chen and Q. Ye, *Dyes and Pigments*, 2019, **165**, 200-211.
26. Y. Wang, Y. Jiang, D. Liu, Y. Wang, G. Wang and J. Hua, *Applied Physics B*, 2018, **124**, 98.
27. H. Xiao, N. Ding, T. Wei, Y. Zhang, X. Zhang and B. Li, *Sensors and Actuators B: Chemical*, 2015, **210**, 204-210.
28. R. Feng, Y. Sun, M. Tian, G. Zhang, R. Zhang, L. Guo, X. Li, X. Yu and N. Zhao, *Journal of Materials Chemistry B*, 2015, **3**, 8644-8649.
29. M. Tasior, I. Bald, I. Deperasińska, P. J. Cywiński and D. T. Gryko, *Org Biomol Chem*, 2015, **13**, 11714-11720.
30. J.-P. Malval, S. Achelle, L. Bodiou, A. Spangenberg, L. C. Gomez, O. Soppera and F. R.-l. Guen, *Journal of Materials Chemistry C*, 2014, **2**, 7869-7880.
31. M. Tasior, V. Hugues, M. Blanchard-Desce and D. T. Gryko, *Asian Journal of Organic Chemistry*, 2013, **2**, 669-673.
32. L. Yan, X. Chen, Q. He, Y. Wang, X. Wang, Q. Guo, F. Bai, A. Xia, D. Aumiler, S. Vdović and S. Lin, *The Journal of Physical Chemistry A*, 2012, **116**, 8693-8705.
33. E. Maçôas, G. Marcelo, S. Pinto, T. Cañeque, A. M. Cuadro, J. J. Vaquero and J. M. G. Martinho, *Chemical Communications*, 2011, **47**, 7374-7376.
34. K. Belfield, M. Bondar, A. Morales, L. Padilha, O. Przhonska and X. Wang, *Chemphyschem : a European journal of chemical physics and physical chemistry*, 2011, **12 15**, 2755-2762.
35. J. C. Collings, S.-Y. Poon, C. Le Droumaguet, M. Charlot, C. Katan, L.-O. Pålsson, A. Beeby, J. A. Mosely, H. M. Kaiser, D. Kaufmann, W.-Y. Wong, M. Blanchard-Desce and T. B. Marder, *Chemistry – A European Journal*, 2009, **15**, 198-208.
36. D. Cao, Z. Liu, Y. Deng, G. Li and G. Zhang, *Dyes and Pigments*, 2009, **83**, 348-353.
37. Z. Liu, P. Shao, Z. Huang, B. Liu, T. Chen and J. Qin, *Chemical Communications*, 2008, 2260-2262.
38. J.-F. Xing, W.-Q. Chen, J. Gu, X.-Z. Dong, N. Takeyasu, T. Tanaka, X.-M. Duan and S. Kawata, *Journal of Materials Chemistry*, 2007, **17**, 1433-1438.